Modulation of orthogonal body waves enables high maneuverability in sidewinding locomotion

Henry C. Astley[a,1], Chaohui Gong[b], Jin Dai[b], Matthew Travers[b], Miguel M. Serrano[a], Patricio A. Vela[a], Howie Choset[b], Joseph R. Mendelson III[a,c], David L. Hu[a], and Daniel I. Goldman[a]

[a]Georgia Institute of Technology, Atlanta, GA 30332; [b]Carnegie Mellon University, Pittsburgh, PA 15213; and [c]Zoo Atlanta, Atlanta, GA 30315

Edited by Michael J. Shelley, New York University, New York, NY, and accepted by the Editorial Board February 20, 2015 (received for review October 1, 2014)

Many organisms move using traveling waves of body undulation, and most work has focused on single-plane undulations in fluids. Less attention has been paid to multiplane undulations, which are particularly important in terrestrial environments where vertical undulations can regulate substrate contact. A seemingly complex mode of snake locomotion, sidewinding, can be described by the superposition of two waves: horizontal and vertical body waves with a phase difference of ±90°. We demonstrate that the high maneuverability displayed by sidewinder rattlesnakes (*Crotalus cerastes*) emerges from the animal's ability to independently modulate these waves. Sidewinder rattlesnakes used two distinct turning methods, which we term differential turning (26° change in orientation per wave cycle) and reversal turning (89°). Observations of the snakes suggested that during differential turning the animals imposed an amplitude modulation in the horizontal wave whereas in reversal turning they shifted the phase of the vertical wave by 180°. We tested these mechanisms using a multimodule snake robot as a physical model, successfully generating differential and reversal turning with performance comparable to that of the organisms. Further manipulations of the two-wave system revealed a third turning mode, frequency turning, not observed in biological snakes, which produced large (127°) in-place turns. The two-wave system thus functions as a template (a targeted motor pattern) that enables complex behaviors in a high-degree-of-freedom system to emerge from relatively simple modulations to a basic pattern. Our study reveals the utility of templates in understanding the control of biological movement as well as in developing control schemes for limbless robots.

sidewinder | biomechanics | robotics | template | control

Propagating waves of flexion along the axis of a long, slender body (henceforth "axial waves") to produce propulsion is common in biological locomotion in aquatic and terrestrial environments. The majority of biological studies of axial wave propulsion at different scales have occurred in aquatic environments (1, 2). Understanding the efficacy of given wave patterns—which are often assumed to act in a single plane (e.g., mediolateral axial bending)—can be gained through full solution of the equations of hydrodynamics (3) or approximations (4). Terrestrial environments such as sand, mud, and cluttered heterogeneous substrates encountered by limbless axial undulators such as snakes can display similar (if not greater) complexity, yet far less attention has been paid to such locomotion (5, 6).

Snake axial propulsion in terrestrial environments differs from fluid locomotion in two key ways. First, most substrates are not yet described at the level of fluids (7), making it a challenge to understand how substrate–body interactions affect locomotor performance, and therefore requiring robotic physical models. Second, the body may be both laterally and/or dorsoventrally flexed (5) to allow different elements of the body to contact (or clear) the substrate and thereby control friction, drag, and substrate reaction forces. Recently progress has been made in understanding how multiplane control allows effective limbless terrestrial locomotion. In studies of laterally undulating snakes (8), a single-plane frictional force model (with drag anisotropy assumed to result from the frictional anisotropy in snake scales) proved insufficient to predict the lateral undulation locomotion performance of these snakes. The authors proposed, modeled, and visualized a mechanism of "dynamic balancing" in which regions of the body with small curvature were preferentially loaded; the addition of this mechanism to their model improved agreement with experiment.

A peculiar gait called sidewinding provides an excellent example of the importance of multiplane wave movement in certain snakes (5, 9). During sidewinding alternating sections of the body are cyclically lifted from the substrate, moved forward via lateral axial waves, and placed into static contact with the substrate at a new location (Fig. 1 *A* and *B*). Owing to the vertical undulatory wave, which controls lifting and contact, the snake can minimize or eliminate drag forces on nonpropulsive portions of the body (Fig. 1*B*), thereby enabling minimal slip at other segments and potentially contributing to a low cost of transport (10). This makes sidewinding particularly attractive to explore aspects of multiplane undulation because lifting perpendicular to the plane of the main axial wave is clearly observable and fundamental to this mode of locomotion (5); failure to lift results in locomotor failure in other vipers (9). In addition, field observations show that sidewinders are remarkably maneuverable, capable of rapidly making large direction changes to elude capture.

Another advantage to studying sidewinding is the existence of a snake-like robot capable of performing effective sidewinding locomotion; our previous robot experiments using this "physical

Significance

We examined the turning behavior of snakes performing sidewinding locomotion using a hypothesized two-wave control template. Sidewinders achieved exceptional maneuverability using two types of turns, shallow differential turns and sharp reversal turns, which we hypothesized are controlled by modulating horizontal wave amplitude and vertical wave phase offset, respectively. We tested these hypothesized control schemes using a modular snake robot capable of sidewinding, resulting in similar behaviors, and explored two-wave parameter space, resulting in discovery of a third turning mechanism that is not seen in snakes. Thus, we show that complex behaviors such as turning while sidewinding can emerge from independent modulations of each of the two waves comprising this control template, underscoring the utility of robots to test biological hypotheses.

Author contributions: H.C.A., H.C., J.R.M., D.L.H., and D.I.G. designed research; H.C.A., C.G., J.D., M.T., and J.R.M. performed research; H.C. contributed new reagents/analytic tools; H.C.A., C.G., J.D., M.M.S., and P.A.V. analyzed data; and H.C.A., C.G., J.D., M.T., M.M.S., P.A.V., H.C., J.R.M., D.L.H., and D.I.G. wrote the paper.

The authors declare no conflict of interest.

This article is a PNAS Direct Submission. M.J.S. is a guest editor invited by the Editorial Board.

See Commentary on page 5870.

[1]To whom correspondence should be addressed. Email: henry.astley@physics.gatech.edu.

This article contains supporting information online at www.pnas.org/lookup/suppl/doi:10.1073/pnas.1418965112/-/DCSupplemental.

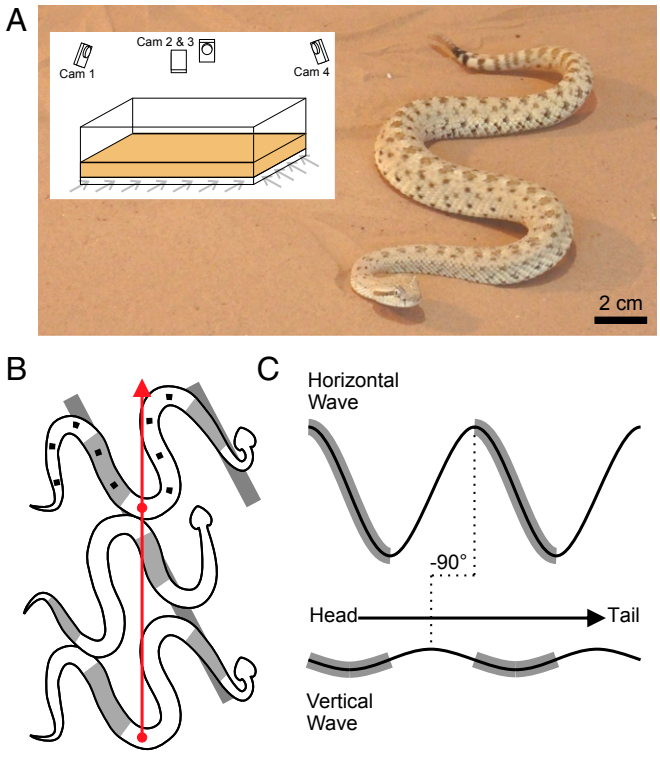

Fig. 1. Sidewinding in *C. cerastes*. (*A*) A sidewinder rattlesnake (*C. cerastes*) performs sidewinding locomotion on sand. (*Inset*) A 1- × 2-m fluidized bed trackway filled with sand from the capture locality (Yuma, Arizona); gray arrows indicate airflow used to reset the granular surface using a fluidized bed (see *Materials and Methods*). (*B*) A diagram of sidewinding in a snake. Gray regions on the snake's body indicate regions of static contact with the ground, whereas white regions are lifted and moving. Tracks are shown in gray rectangles. Points on the final snake indicate approximate marker locations used in our experiments. The red arrow indicates direction of motion of the estimated center of mass. (*C*) Horizontal and vertical body waves during straight sidewinding with the head to the right, as seen in *A* and *B*, offset by a phase difference (ϕ) of −90°. Gray regions indicate static contact. The arrow depicts the posterior propagation of waves down the body. Although depicted as sinusoidal waves here, the waves may (and often do) have other forms.

model" (9) revealed that despite the anatomical complexity associated with hundreds of body elements and thousands of muscles (11) biological sidewinding could be simply modeled as a combination of two axial waves: horizontal and vertical axial waves with identical spatial and temporal frequency but different amplitudes offset by a phase difference (ϕ) of ±90° (Fig. 1*C*) (9). Using this scheme, we showed that sidewinders ascend granular inclines by modulating the vertical wave amplitude to control contact length, and implementing this strategy in a snake robot allowed the device to ascend similar inclines (9). We proposed more broadly that the appropriate modulation of the two waves was in fact a control "template," defined as a behavior that contains the smallest number of variables and parameters that exhibits a behavior of interest (12). Templates provide relatively simple targets for motion control and feedback responses (13) and have proved useful to understand locomotion of legged runners (14), climbers (15), and undulatory swimmers (16).

In this paper, we make the first systematic observations of turning behaviors in sidewinder rattlesnakes then show that the seemingly complex turning behaviors can be explained as modulations of the template by applying these modulations of our robotic physical model. This reveals both that the two-wave template describes the motions of the animal and that maneuvers can be achieved through independent amplitude and phase modulation of the two waves. We also go beyond biological observations to generate maneuvers on the robot that are not observed in the animals.

Results and Discussion

Snake Turning. Sidewinder rattlesnakes used two discrete turning mechanisms to change direction on sand, which we termed "differential" and "reversal" turns (Fig. 2 and Movies S1 and S2). Differential turns were shallow (mean ± SD: 26.3° ± 18.3° per cycle, maximum: 66.9°) but could continue for many cycles (Fig. 2 *A* and *C* and Movie S1), whereas reversal turns were sudden, sharp turns (89.4°± 28.2° per cycle, maximum: 176.6°) (Fig. 2 *B* and *C* and Movie S2). Both reversals and differential turns occurred regardless of movements of the experimenters outside the area (a possible perceived threat), although qualitative assessment suggested that reversals were a more common response to vigorous movements of experimenters.

Two of the variables examined (*Materials and Methods*) give crucial insights into the underlying control of these behaviors. During differential turns, the distance moved by body segments farthest from the center of rotation (d_1, Fig. 3*A*) was greater than the distance moved by body segments closest to the center of rotation (d_2, Fig. 3*A*) per cycle. When normalized by postural width (L, Fig. 3*A*), this difference in movement distance ($|d_1 - d_2|/L$) was proportional to the change in direction per cycle (Fig. 3*C*). Furthermore, this relationship was close to the theoretical prediction based on differential drive vehicles (*Materials and Methods*). Differential turns in which the anterior of the snake was closest to d_1 (Figs. 2*A* and 3*C*) were more common than differential turns in which the head was closest to d_2, but there was no difference in turn angle per cycle. In contrast, reversal turns displayed a discontinuous

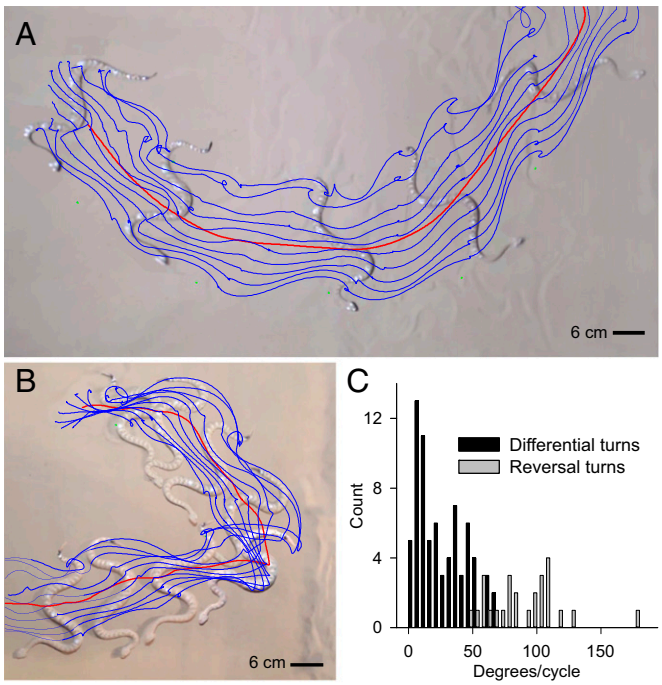

Fig. 2. Turning behaviors of sidewinder rattlesnakes. (*A*) Differential turning, shown here using composite frames from overhead video. Blue lines indicate the path of points along the body, and the red line is the path of the approximate center of mass. (*B*) Reversal turning, shown here using composite frames from overhead video and point paths as in *A*. (*C*) Histogram of turn magnitude (change in direction per cycle) for differential and reversal turns. Differential turns resulted in lower changes in direction per cycle than reversal turns, although there was some overlap.

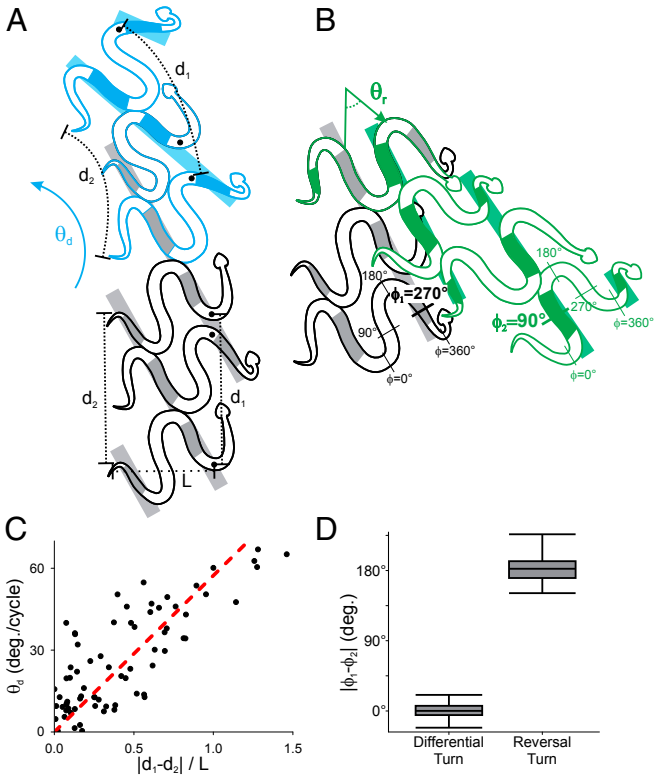

Fig. 3. Kinematics and hypothesized mechanics of turning behaviors. (*A*) A diagram of straight sidewinding (gray) followed by differential turning (blue), with the snake turning toward the top left of the page at θ_d degrees per cycle (change in orientation of the approximate center of mass velocity vector). The arc-length distance moved per cycle is d_1 for the head and d_2 for the tail, although these are reversed when the head is on the inside of the turn, and postural width is L. (*B*) A diagram of straight sidewinding (gray) followed by reversal turning (green), with the snake turning toward the bottom right of the page at θ_r degrees per cycle. When viewed relative to the direction of motion, the head is initially to the right of the snake's body, but it is on the left after the reversal turn. (*C*) Rate of differential turning correlates significantly with displacement difference normalized by length $|d_1 - d_2|/\mathrm{L}$ ($r^2 = 0.53$, $P < 0.0001$), with a slope statistically indistinguishable from the theoretical prediction (red line). (*D*) Difference in horizontal wave phase of the static regions of the snake before and after the turn. The phase changes by almost exactly 180° in reversal turns but does not change in either differential turns or straight locomotion.

phase shift ($|\phi_1 - \phi_2|$) of 180° ± 20° (Fig. 3*B*), compared with 1° ± 11° in differential turning and straight sidewinding (Fig. 3*D*).

Reversal turning represents a novel method of turning, without a direct analog in limbed locomotion. During a reversal, the body segments that are in static contact with the ground ("stance phase") switch roles with body segments previously moving above the substrate ("swing phase"), without the horizontal wave changing in shape or propagation direction. This is in contrast to the possibility of changing direction by switching the wave propagation direction, like a wheeled vehicle moving in reverse; sidewinders have not been observed to generate anteriorly propagating waves and may lack the ability to do so. Because of the shape of the horizontal body wave (Fig. 1*B*), the moving and static segments [at phases +90° and −90° (Fig. 3*B*)] will be at a relatively shallow angle (40.4° ± 17.4°), but moving in opposite directions relative to the snake's center of mass. The phase shift of a reversal turn will cause these segments to swap roles, and consequently the direction of motion of ground-contact segments will change dramatically, allowing the snake to suddenly move in a different direction. Additional reorientation movements may occur before the resumption of movement, giving rise to the observed range of reversal turn angles (Fig. 2*C*) and producing a variety of values of $|d_1 - d_2|/\mathrm{L}$. Furthermore, because snakes use sidewinding with a vertical wave phase offset of either 90° or −90° without apparent behavioral preference or locomotor performance difference during straight sidewinding, using a reversal turn to switch between these two vertical wave phase offsets should incur no reduction in performance (Dataset S1). In contrast, limbed organisms attempting to change direction without reorientation by simply walking backward may find their limbs ill-suited to this new direction.

In most animals, turning requires both changing the direction of motion and reorienting the body correspondingly (17), and only a few are capable of turns without reorientation or locomotor decrement [e.g., brittle stars (18)]. Additionally, the sharp direction change in reversal turning (Fig. 2), without obvious kinematic predictors like the displacement gradient in differential turning (Dataset S2), may make anticipating the snake's movements more difficult for predators. This evasive capability, along with the general speed and economy of sidewinding locomotion, may be a critical component in allowing the long-distance movements of sidewinders across exposed terrain (19). Both turning modes can be used sequentially by the snakes, with four analyzed trials showing a differential turn before or after a reversal (Fig. S1), allowing a wide range of versatile turning behaviors and reorientations on the yielding granular substrate.

Testing Turning Templates in a Physical Robotic Model. Based on these results, we propose the following modulations of the two-wave template for differential and reversal turning: Differential turning should occur in the robot when the amplitude of the horizontal wave changes along the body, such that the wave either increases or decreases amplitude as it propagates posteriorly (Fig. 4*C*). This is broadly similar to the previously developed robot conical turning mechanism (20) but without a corresponding increase in vertical wave amplitude. Reversals were implemented in the robot via a sudden 180° phase shift in the vertical wave (Fig. 4*D*), effectively reversing the "handedness" of the elliptical helix (left-handed versus right-handed) used to specify segment positions, such that ground contact versus elevated segments switched roles.

To test these hypothesized two-wave template modulations, we used a physical model: a modular limbless robot (Fig. 4 *A* and *B*) that, through application of the two-wave template, produces sidewinding locomotion similar to biological snakes. We applied our hypothesized turning templates to the snake robot while it moved in a sand arena and achieved both types of turning (Fig. 4 and Movies S3 and S4). The differential turning mechanism produced effective but gradual turning (Fig. 4 *E* and *G* and Fig. S2) of a magnitude similar to that of the snake (Dataset S3), although limitations of joint angles and resolutions prevent higher turn angles for the robot. This resulted in greater forward displacement per cycle at the end of the robot on the outside of the curve, similar to the snake and the theoretical prediction line (Fig. 4*G*). The reversal turning mechanism produced sharp turns (170.1°± 3.6°, maximum: 174.5°) (Fig. 4*F* and Fig. S2) of even greater magnitude than in snakes (Dataset S3). Applying these mechanisms on hard ground produced similar behaviors, suggesting that the limited slip of sidewinding and associated turning mechanisms provide versatile locomotion across substrates.

These results demonstrate the utility of robots as physical models for testing hypothesized mechanisms underlying locomotor behavior. Although robots only crudely approximate the morphology and behavior of an animal, if they rely upon the same overall mechanics to achieve locomotion they can display similar locomotor responses to changes in waveform or the environment. This particular robot displays not only kinematics and sidewinding locomotion that are similar to those of biological

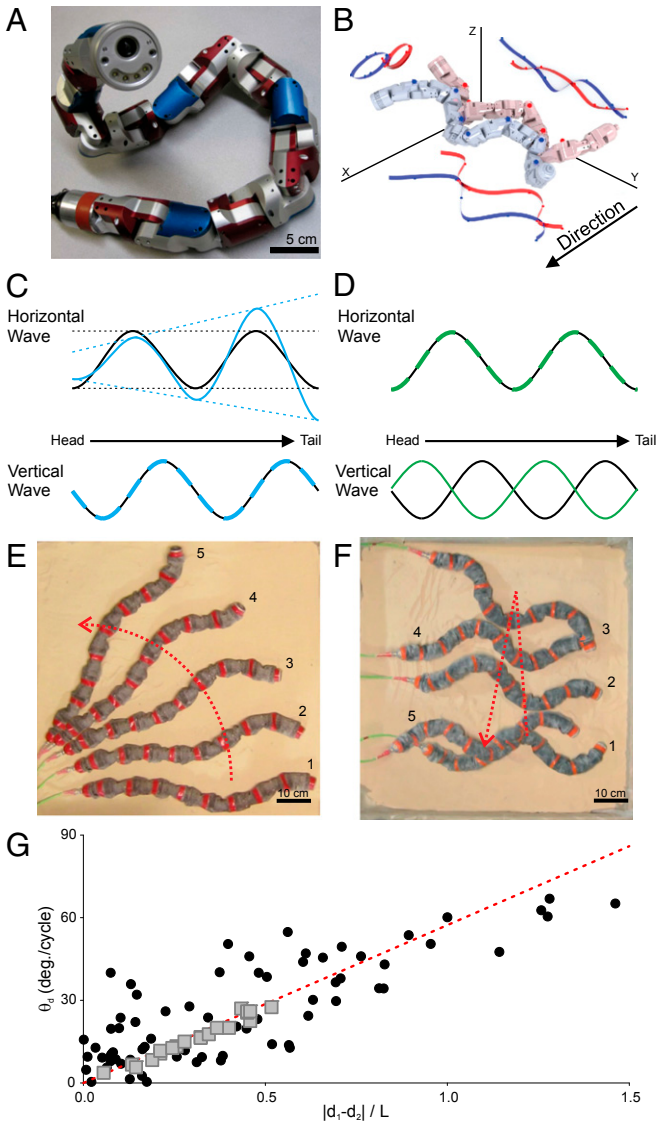

Fig. 4. Robot motions produced by hypothesized turning mechanisms. (*A*) A 16-joint snake robot capable of sidewinding. (*B*) Two sequential renderings of the robot during sidewinding, in which the robot adopts an elliptical helix posture produced by the sum of horizontal and vertical sine waves with a ±90° phase difference. Both waves propagate posteriorly, resulting in cyclic, posteriorly propagating regions of lifted movement and static ground contact, without rolling, as in biological sidewinding. (*C*) Horizontal and vertical waves of the robot during normal sidewinding (black) and differential sidewinding (blue). (*D*) Horizontal and vertical waves of the robot during normal sidewinding (black) and immediately following reversal turning (green). (*E*) Differential turning in the robot, shown here using composite frames from overhead video over 17 seconds. The red line indicates the approximate path of the center of mass. (*F*) Reversal turning in the robot, shown here using composite frames from overhead video over 30 seconds and center of mass path as in *E*. (*G*) Comparison of snake (black circles) and robot (gray squares) differential turning with theoretical predictions (red line). Limitations of joint angles and resolutions prevent higher $|d_1 - d_2|/L$ values for the robot.

snakes but can use control strategies used by snakes sidewinding on inclined sand to achieve performance similar to that of the snakes (9), suggesting that the robot's responses and fundamental mechanics are sufficiently similar to be a good physical model. Thus, we cannot only show significant kinematic differences between each turn type and straight sidewinding but also can show that these mechanisms, in isolation, will produce similar behaviors in the robot. Thus, our physical robot model provides strong evidence that these hypothesized mechanisms are the cause of turning in biological snakes, rather than correlates of undetected mechanisms.

Both mechanisms are modulations of the two-wave model, which suggests it is indeed a neuromechanical template (21) that the organisms use to coordinate their locomotion, as proposed in ref. 9. Whereas these turns constitute a form of internal perturbation, further testing of this hypothesized template should include how the animal responds to external perturbations (22) (such as obstacles) as well as measurements of the underlying neural controls predicted by template control (e.g., as in sand swimming in ref. 23). Coupling such studies to further investigation of the robot could help explain why the sidewinder rattlesnake moves effectively on granular media, whereas its close relatives do not (9), and establish these organisms as an ideal model system for two-wave template locomotion. Additionally, the emergence of complex turning behaviors from the independent modulation of the two waves in this template suggests that the limited variables in a low-dimensional representation of movement do not necessarily limit the organism or robot to simple behaviors. Consequently, templates with similarly independent control dimensions may be beneficial in other systems, including limbed locomotion.

We next explored aspects of the two-wave model parameter space in which the two waves were modulated with respect to each other. Most phase differences other than ±90° produced elliptical helix body postures with nonhorizontal major axes, which immediately toppled and thereby became identical to ±90° phase differences. Phase differences of 0° and 180° produced nonhorizontal planar waves that toppled to become lateral undulation. Differences in relative posterior wave propagation speeds produced an oscillating motion with no net displacement or rotation. However, varying the relative spatial frequency of the vertical and horizontal waves produced a behavior that we term "frequency turning" (Fig. 5). If the vertical wave spatial frequency was set to either 0.6 or 1.3 of that of the horizontal wave, forward displacement per cycle was small and the robot rotated at up to 127° per cycle, almost rotating in place (Fig. 5). During frequency turning, the anterior and posterior ends lifted and rotated in the same direction about the static central segments (Fig. 5*B*, t_1), then each end lowered and formed a rotating anchor point while the central segments raised and reoriented (Fig. 5*B*, t_2), returning the robot to the starting position with

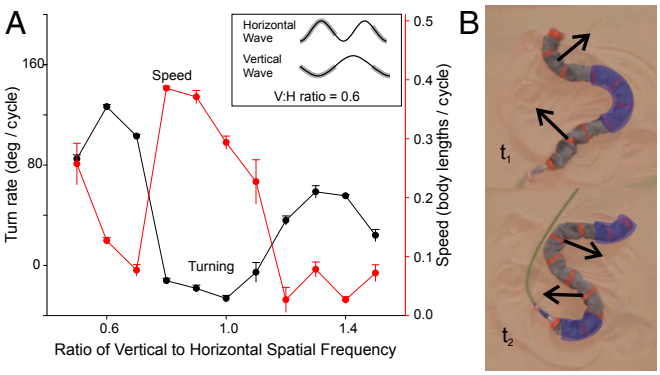

Fig. 5. (*A*) The effect of varying vertical spatial frequency (relative to horizontal frequency) on speed and turning. (*Inset*) The waveform of the horizontal and vertical waves at a ratio of 0.6. Gray regions indicate static contact. (*B*) Two sequential stills 2.3 s apart in Movie S5 of a snake robot performing frequency turning at a ratio of 0.6 (0.14 Hz). Purple-shaded areas are instantaneously static. Black arrows show the direction of motion of moving segments.

minimal translation but substantial rotation (Fig. 5*A*). Frequency turning was not observed in snakes, although it is unknown whether this is due to biological limitations in the nervous or muscular system or simple behavioral preference. This discovery shows the potential for versatile behaviors in wave-mixing control of high-degree-of-freedom systems, as well as highlighting the need for more thorough characterization of parameter space in the future.

Driving a Limbless Robot. In addition to the testing of biological hypotheses associated with neuromechanical control of sidewinding and turning using a mixture of two waves, this framework has practical applications regarding steering a snake robot. No previous snake robot controller can command a snake robot to follow an arbitrary path, owing to the need for a sophisticated dynamic model and difficult-to-tune motion controller (24). With the two-wave mixing framework, however, steering a snake robot is simplified to adjusting only a few wave parameters, and the straightforward correspondence between the parameter value and the resultant behaviors allows intuitive high-level motion control of the robot. For example, the amplitude gradient in differential turning corresponds to the "steering" of a wheeled vehicle and the wave speed directly relates to the speed of "driving." Fig. 6 demonstrates the robot being joystick-driven by a human in a test course using the two-wave control method (*Materials and Methods*).

Conclusions

Sidewinder rattlesnakes turned using two distinct mechanisms, shallow differential turning and sharp reversal turning. The differential mode allowed gradual turning across a number of cycles, whereas the reversal mode resulted in sudden and larger changes in direction without body rotation. We demonstrated that such turns could be elicited in a physical robot model through suitable modulation of two waves: the horizontal body wave amplitude or vertical body wave relative phase, respectively. This supports our hypothesis that snakes generate sidewinding through a two-wave neuromechanical (21) control template, and that turns are produced by modulations of this template. The independent modulation of control axes (e.g., axial waves) allows for the emergence of complex behaviors from low-dimensional representations and may be a common feature across these control systems, making terrestrial locomotion of snakes an excellent system for understanding the generation of complex motions from simple templates. Practically, our results demonstrate that the two-wave mixing scheme offers a significant advance in the control of limbless snake-like robots (which already show promise for use in challenging environments such as urban search and rescue), greatly expanding their maneuverability and simplifying user control. Discovery of such templates promises advances in use of robots in complex and unpredictable real-world environments without computationally demanding planning and control of each independent joint. For example, adherence to a template could make the locomotion robust to changes in substrate conditions, simplifying necessary control with the need to only slightly modulate a parameter in one of the waves.

Materials and Methods

Snakes. We used four adult sidewinder rattlesnakes (*Crotalus cerastes*) (Fig. 1*A*) (Dataset S4) collected near Yuma, Arizona and housed at Zoo Atlanta. Testing was conducted at air and sand temperatures of 21–25 °C, comparable to the field-active temperatures of this species (25). All procedures were approved by both Georgia Institute of Technology and Zoo Atlanta Institutional Animal Care and Use Committees, and antivenom was stocked at the nearest hospital.

Snake Turning Trials. All turning trials were conducted in a horizontal 1- × 2-m^2 fluidized bed filled with sand collected from the capture locality (Fig. 1*A*) (9). Air is driven through a rigid porous plate beneath the sand to fluidize the sand, erasing tracks and returning the bed to a uniform compaction state with level sand between trials (during which airflow is off). We attempted to minimize snakes crossing their own tracks during trials, although no effect was noticeable when such crossings occurred, and it was unavoidable in particularly sharp reversals. Test duration was limited (<10 min) and interspersed with equal or greater rest periods to prevent fatigue, with no more than three tests per snake per day. Recorded movement sequences were discarded if snakes stopped, interacted with walls, or turned within one period of the start or end of a sequence.

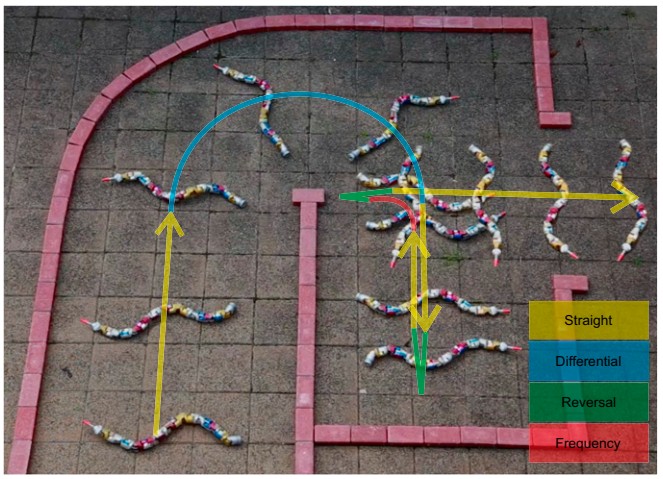

Fig. 6. Images from Movie S6 showing the sidewinder robot moving through a trackway using three turn types (labeled) and straight-line sidewinding. The size of the test course is 3 × 3 m^2 and the robot completed the course in 48 s.

Snake Tracking and Image Processing. The anterior one-fourth of the snake was restrained in a tube by keepers while 5-mm^2-square patches of reflective tape were adhered to the remainder of the body at ∼5-cm intervals, with the last two markers at the vent and base of the rattle (Fig. 1*B*). The more anterior portions of the snake could not be safely marked. Three-dimensional marker motions were recorded with four calibrated infrared motion-capture cameras at 120 frames per second (Optitrack Flex 13; Natural Point, Inc.) using Motive software (v 1.5; Natural Point, Inc.). Point identities were not always maintained throughout a sequence, so the tracked positions were considered to be detections and the correspondences (and thus trajectories) were managed using a Kalman–Munkres formulation.

Penalized B-splines (26) were used to model the geometry of the snake's body. The B-splines formulation fits a polynomial function to the data points by minimizing the error term $E=\frac{1}{2}\|X(s,t)-\Phi^n(s)\alpha(t)\|^2+\lambda\alpha(t)^T\nabla^2\alpha(t)$, where $\Phi^n(s)=[\phi_1^n(s)\,\phi_2^n(s)\,\ldots\,\phi_m^n(s)]$ is a matrix constructed by the n^{th}-order B-spline basis functions, and $\alpha(t)=[\alpha_1(t)\,\alpha_2(t)\,\ldots\,\alpha_m(t)]^T$ are the corresponding coefficients or control points. ∇^2 is the Laplacian operator, m is the number of basis points used, s is the parameterization along the length of the body, t denotes time, and λ is the regularization term. Reconstruction of the curve $f(s,t)$ is accomplished with the function, $f(s,t)=\Phi^n(s)\alpha(t)$.

For this application one basis function was used for every marker tracked. Minimizing the error function with respect to α leads to a least-squares solution with soft curvature constraints imposed by the regularization term. Furthermore, to capture the range of motions the snakes could achieve the model should only apply soft constraints. A benefit of the B-splines model is that the fitting basis functions $f\Phi(s)$ have only local support, thereby preventing points that are spatially distant from influencing each other significantly during fitting. For example, the fitting of the curve near the head will not be influenced by the fitting of the curve near the tail.

An approximate center of mass was defined as the average location of all spline points, which was used to compute overall velocity and turn angle per cycle. Cycles were delimited based on the initiation and cessation of motion of the most anterior point, with the cycles during straight and differential turning defined by two subsequent initiations of movement. Owing to the phase shift during reversals, which would cause previously moving points to become static, cycles were defined as a period including three such initiation or cessation events. Each run, depending on period and duration, could

contain anywhere between one and three complete periods of movement for analysis.

Displacement gradient per cycle $(d_1 - d_2)$ was calculated as the difference between the line integrals of third-order polynomial curves approximating the paths of the most anterior and posterior points, then normalized by postural distance between them (L). The theoretical prediction for differential turning is based on analogy to a differential-drive vehicle. The nonuniform amplitude in the horizontal wave causes one end moving faster than the other and, as a result, a snake changes its direction of motion. Let $\dot{d}_1$ and $\dot{d}_2$ denote the instantaneous velocities (orthogonal to the wave axis) of the most anterior and posterior markers on the snake. The angular velocity of the snake about the vertical world-space axis is computed as $\dot{\theta}_t = (\dot{d}_1 - \dot{d}_2)/L$ where L is the distance between the two markers along the wave axis. Integrating $\dot{\theta}_t$ over a gait cycle, the net change of orientation is $\Delta\theta_t = \int(\dot{d}_1 - \dot{d}_2)/L dt = (d_1 - d_2)/L$, or in degrees $\Delta\theta_t = \frac{180}{\pi}(d_1 - d_2)/L$.

Although other measures of waveform were computed, such as half-wavelength, angle between bends, percent static contact, and average amplitude, none was significantly different between turn types or from straight-line sidewinding, and none correlated with turn angle, and thus they are not considered further. Turns were categorized as reversals or differentials, with turns of less than 10° being considered straight for some statistical analysis (this did not alter the overall conclusions compared with the simpler differential versus reversal categorization). The effect of turning type was determined using a mixed-model full-crossed ANOVA, with turn type as a fixed factor and individual as a random factor; all F and P values for all factors and variables are given in Dataset S2. To determine whether variables displayed correlated changes to turn angle, a series of regressions were performed between the variables an turn angle, separated into reversal and differential turns (Dataset S5). To determine whether body shape and velocity differed before and after a reversal, we performed a series of two-tailed paired t tests (Dataset S1).

To determine whether a point is static or moving, despite limited vertical data resolution and low ground clearance, we applied a threshold based on velocity distribution throughout the trial; across all trials, the average fraction of the body that was stopped was 44%, which did not differ across types of turns and straight sidewinding. To assess the phase of the horizontal wave, we quantified the curvature and rate of curvature change for all points along the body. The phase of the static regions for a given time was defined as the mean and 95% confidence interval of the phase of all static points (to exclude outliers), with the mean assumed to represent the lowest point in the vertical wave for the purposes of calculating the phase offset between horizontal and vertical waves. The total static region was typically 168° ± 42° across trials. To assess the possible phase shift $(|\phi_1 - \phi_2|)$ during turning, we used the difference between the mean static phase before and after turns. Across all trials, mean static phase showed a nearly perfect bimodal distribution, with 90 trials showing a mean static phase of approximately 90° (87° ± 9°) and 106 of approximately 270° (= −90°) (267° ± 10°), indicating a similar prevalence of sidewinding with the head on the right and left of the snake.

Robot Turning Trials. Hypothesized turning mechanisms were tested using a modular snake robot consisting of 16 joints, alternating between vertical and horizontal bending, thereby allowing a wide range of postures (27) (total length: 94 cm, mass: 3,150 g) (Fig. 4*A*). Straight-line motion was produced by two posteriorly traveling waves (of the same spatial frequency) in the horizontal and vertical planes (9) with a phase offset of ±90° (Fig. 4*B*). Reversal turning was produced by shifting the vertical wave by a phase of 180° and differential turning was achieved by superimposing an amplitude gradient to the horizontal wave in straight-line sidewinding (20). The robot was then placed in a sand-filled arena, and the resulting behavior was evaluated based on motion capture from overhead video recording. To compare turn magnitude per cycle of the robot and snake, we performed an ANOVA with turn type and robot versus snake as fixed, crossed factors (Dataset S3).

We evaluated the efficacy of the two-wave mixing framework to control the robot motion on a test course (Fig. 6). Frequency turning was implemented by setting the spatial frequency of the vertical wave 0.6 times of the horizontal wave and keeping everything else identical to straight-line sidewinding. A human operator used a set of buttons to switch between different motions and used a joystick to continuously vary the amplitude gradient of differential turning. Straight-line sidewinding was used to follow a straight path. When the robot deviated from a path or when it was following a curve, the human operator used the joystick to regulate the amplitude gradient of differential turning to keep the robot along the path. When a tight turn was required, the operator switched to frequency turning to quickly reorient the robot. Reversal turning was triggered when the robot hit the dead end and reversed its moving direction.

ACKNOWLEDGMENTS. The authors thank Hamidreza Marvi, Weikun Zhen, Luke Buffardi, Jason Brock, Robert Hill, David Brothers, and Wade Carruth for their valuable assistance. This research was supported by National Science Foundation (NSF) Grants 1150760, ECCS-0846750, and 0848894; NSF funding for the Student Research Network in the Physics of Living Systems Grant 1205878; Army Research Office Grant W911NF1010343; and the Georgia Institute of Technology School of Biology and Elizabeth Smithgall Watts endowment. Research was sponsored by the Army Research Laboratory and was accomplished under Cooperative Agreement No. W9llNF-l0-2-0016. The views and conclusions contained in this document are those of the authors and should not be interpreted as representing the official policies, either expressed or implied, of the Army Research Laboratory or the US Government. The US Government is authorized to reproduce and distribute reprints for Government purposes not withstanding any copyright notation herein.

1. Webb PW, Blake RW (1985) Swimming. *Functional Vertebrate Morphology*, eds Hildebrand M, Bramble DM, Liem KF, Wake DB (Harvard Univ Press, Cambridge, MA), pp 110–128.
2. Stephens GJ, Johnson-Kerner B, Bialek W, Ryu WS (2008) Dimensionality and dynamics in the behavior of *C. elegans*. *PLoS Comput Biol* 4(4):e1000028.
3. Tytell ED, Hsu CY, Williams TL, Cohen AH, Fauci LJ (2010) Interactions between internal forces, body stiffness, and fluid environment in a neuromechanical model of lamprey swimming. *Proc Natl Acad Sci USA* 107(46):19832–19837.
4. Taylor G (1952) Analysis of the swimming of long and narrow animals. *Proc R Soc Lond A Math Phys Sci* 214(1117):158–183.
5. Jayne BC (1986) Kinematics of terrestrial snake locomotion. *Copeia* 1986:195–208.
6. Sharpe SS, et al. (2015) Locomotor benefits of being a slender and slick sand-swimmer. *J Exp Biol* 218:440–450.
7. Goldman DI (2014) Colloquium: Biophysical principles of undulatory self-propulsion in granular media. *Rev Mod Phys* 86(3):943. (abstr).
8. Hu DL, Nirody J, Scott T, Shelley MJ (2009) The mechanics of slithering locomotion. *Proc Natl Acad Sci USA* 106(25):10081–10085.
9. Marvi H, et al. (2014) Sidewinding with minimal slip: Snake and robot ascent of sandy slopes. *Science* 346(6206):224–229.
10. Secor SM, Jayne BC, Bennett AF (1992) Locomotor performance and energetic cost of sidewinding by the snake crotalus cerastes. *J Exp Biol* 163:1–14.
11. Gasc JP (1981) Axial musculature. *Biology of the Reptilia* (1981) Vol 11:355–435.
12. Holmes P, Full RJ, Koditschek D, Guckenheimer J (2006) The dynamics of legged locomotion: Models, analyses, and challenges. *SIAM Rev* 48(2):207–304.
13. Full RJ, Koditschek DE (1999) Templates and anchors: Neuromechanical hypotheses of legged locomotion on land. *J Exp Biol* 202(Pt 23):3325–3332.
14. Cowan NJ, Lee J, Full RJ (2006) Task-level control of rapid wall following in the American cockroach. *J Exp Biol* 209(Pt 9):1617–1629.
15. Goldman DI, Chen TS, Dudek DM, Full RJ (2006) Dynamics of rapid vertical climbing in cockroaches reveals a template. *J Exp Biol* 209(Pt 15):2990–3000.
16. Ding Y, Sharpe SS, Wiesenfeld K, Goldman DI (2013) Emergence of the advancing neuromechanical phase in a resistive force dominated medium. *Proc Natl Acad Sci USA* 110(25):10123–10128.
17. Jindrich DL, Full RJ (1999) Many-legged maneuverability: Dynamics of turning in hexapods. *J Exp Biol* 202(Pt 12):1603–1623.
18. Astley HC (2012) Getting around when you're round: quantitative analysis of the locomotion of the blunt-spined brittle star, Ophiocoma echinata. *J Exp Biol* 215(Pt 11): 1923–1929.
19. Secor SM (1994) Ecological significance of movements and activity range for the sidewinder, crotalus cerastes. *Copeia* 1994:631–645.
20. Gong C, Hatton RL, Choset H (2012) Conical sidewinding. *Proceedings of the 2012 IEEE International Conference on Robotics and Automation* (IEEE, New York).
21. Nishikawa K, et al. (2007) Neuromechanics: An integrative approach for understanding motor control. *Integr Comp Biol* 47(1):16–54.
22. Jindrich DL, Full RJ (2002) Dynamic stabilization of rapid hexapedal locomotion. *J Exp Biol* 205(Pt 18):2803–2823.
23. Sharpe SS, Ding Y, Goldman DI (2013) Environmental interaction influences muscle activation strategy during sand-swimming in the sandfish lizard Scincus scincus. *J Exp Biol* 216(Pt 2):260–274.
24. Liljeback P, Haugstuen IU, Pettersen KY (2012) Path following control of planar snake robots using a cascaded approach. *Control Systems Technol* 20(1):111–126.
25. Secor SM, Nagy KA (1994) Bioenergetic correlates of foraging mode for the snakes crotalus cerastes and masticophis flagellum. *Ecology* 75:1600–1614.
26. Eilers PHC, Marx BD (2010) Splines, knots, and penalties. *Wiley Interdisciplinary Reviews: Computational Statistics* 2(6):637–653.
27. Wright C, et al. (2012) Design and architecture of the unified modular snake robot. *Proceedings of the 2012 IEEE International Conference on Robotics and Automation* (IEEE, New York).